Contents list available at CBIORE journal website

International Journal of Renewable Energy Development

Journal homepage: https://ijred.cbiore.id

Research Article

Accurate SRT-BGK model evaluation of heatlines visualization and entropy generation of convective heat transfer inside an inclined U cavity receiver as application of solar thermal energy systems

Taoufik Naffouti[1, 2, 3,4*] and Lamia Thamri[2, 4]

[1] *University of Tunis El-Manar, Faculté des Sciences de Tunis, Département de Physique, Tunis, Tunisia*

[2] *Laboratoire d'Energétique et des Transferts Thermique et Massique, El Manar 2092, Tunis, Tunisia.*

[3] *Institut Préparatoire aux Etudes d'Ingénieurs El-Manar, El-Manar 2092, Tunis, Tunisia.*

[4] *College of Sciences and Humanities of Dawadmi, Shaqra University, Shaqra, Kingdom of Saudi Arabia*

Abstract. The present study analyzes thermal and dynamic fields, heatlines visualization and entropy generation as well as flow energy, flow rate and heat transfer through a natural convection flow inside a top-open cavity receiver. For the case of a horizontal cavity, lower walls are heated at a uniform temperature while vertical walls are treated as adiabatic. The lattice Boltzmann method (LBM) is applied to solve governing equations of the problem. Effects of Rayleigh number ($10^3 \leq Ra \leq 10^5$), cavity orientation ($0° \leq \theta \leq 75$) and cavity aspect ratio ($1 \leq A \leq 1.75$) on thermo-fluid characteristics of the flow are performed. It was found that current findings computed by LBM are in line with existing literature. Findings reveal that flow patterns and heat transfer are strongly affected by variations of Ra, θ and A. The rise of Ra leads to a change in the orientation of heatlines trajectories with a growth of the stratification degree of entropy generation within the horizontal square cavity. Additionally, an enhancement of the convective heat transfer is detected as increasing Ra accompanied with more energy absorbed by the flow and an intensification of the entrainment phenomenon of fresh air by thermal plumes. For $Ra = 5 \cdot 10^4$, the optimization of heat transfer and total entropy generation demonstrate the existence of a critical angle of the square cavity receiver corresponding to the cavity orientation of $\theta = 45°$.Increasingthe angle θ reduces the stratification degree of heatlines and entropy generation as well as the flow rate. The rise of the geometrical parameter A entrains an increase of thermal gradients with a deceleration of the flow circulation. A decrease of flow rate and convective heat transfer with the growth of the aspect ratio of a horizontal cavity is detected for $Ra = 5 \cdot 10^4$.

Keywords:U cavity receiver, LBM, convective heat transfer, heatlines visualization, entropy generation

Received: 14th Nov 2024; Revised: 28th April 2025; Accepted: 29th May 2025; Available online: 29th June 2025

1. Introduction

The convective heat transfer is extensively used in industrial applications owing to simplicity, high reliability, absence of noise and low maintenance costs (Kim and Lee 1996, Peterson and Ortega 1990 and Aydin and Yang 2000). This mode of energy transferin semi-confined cavities relevantto a wide range research and engineering applications, such as design and optimization of solar thermal receivers (Shirvan *et al.* 2017, Loni *et al.* 2018, Pavlovic *et al.* 2018, Nayak *et al.* 2018, Venkatachalam and Cheralathan 2019, Ophoff *et al.* 2020 and Sadat 2022), heat exchanger apparatus (Novozhilova *et al.* 2017, Kumar *el al.* 2017, Unger *et al.* 2019 and Unger *et al.* 2020), solar energy collectors (Huang *et al.* 2013, Ghazouani *et al.* 2019 and Hassan *et al.* 2021), energy storage systems (Tian and Zhao 2013, Liu *et al.* 2018 and Prasad *et al.* 2019), among others.

The solar thermal power technology is attractive owing to efficiency and operational flexibility (Wu *et al.*2012). This technology has already made good progress in commercialization applications, research and development, and so on. Until now, the solar cavity receiver plays a significant role for the conversion of solar thermal energy into electrical energy.

The literature demonstrates that both numerical and experimental investigations have been carried out to exam the propagation of natural convection inside cavity receivers with different geometries via experimental apparatus and computational approaches. Using Lattice Boltzmann method, Haghshenas *et al* (2010) predicted heat transfer and fluid dynamics of a free convection in an open-ended square cavity packed with porous medium. They noted that the increase of Rayleigh number and porosity conducts to an intensification of flow circulation and heat transfer inside the cavity. Then, Fontana *et al* (2011) examined a 2D steady buoyancy-driven flow of air in a square open cavity heated from the bottom by a centred internal hot source while the cold right wall contains a partial opening with different height. Via finite volume CFD commercial package ANSYS CFX, they demonstrated a significant influence of the cavity opening on temperature and flow patterns as well as the heat transfer.

*Corresponding author
Email: taoufiknaffouti@gmail.com (T. Naffouti)

https://doi.org/10.61435/ijred.2025.60842
ISSN: 2252-4940/© 2025.The Author(s). Published by CBIORE

Through the finite volume approach, Mahmoudi *et al.* (2012) investigated the entropy generation of a natural convection in a partially open cavity with a thin heat source subjected to copper-water nanofluid. For the open boundary located up the cavity, the intense flow circulation conducts to an increase of the heat transfer with a decrease of the total entropy generation. Then, McGarry and Kohl (2013) applied finite volume Fluent software to analyse the convective heat transfer in a square enclosure partially open by right vertical boundary and heated from left vertical wall with two heat blocks. For different Rayleigh number ratio, the flow is described by a main vortex centred at the middle of the enclosure with a second vortex located in its corner between heaters. Azwadi *et al.* (2013) examined thermal and dynamic fields of a free convection inside an open-ended rectangular enclosure partially heated by the left vertical wall using lattice Boltzmann method. As increasing the aspect ratio of the enclosure, they founded that the flow structure becomes more symmetrical near its open vertical wall. An attenuation of the average Nusselt number is detected for various positions of heated wall and Grashof numbers. Then, Prakash (2014) analyzed a free convection heat loss from cylindrical solar cavity receivers using Fluent CFD software. A growth of the convective heat losses is noted as increasing the opening ratio of the cavity receiver.

By means of the finite difference method, Bondareva *et al.* (2016) studied the behaviour of the natural convection in an inclined wavy open porous cavity including a nanofluid subjected to a uniform magnetic field. The rectangular cavity open by the top is heated at the right bottom corner with a constant temperature. To visualize the heat transport way, they analysed heatlines of the flow. For a fixed Rayleigh number at 10^3, they concluded that streamlines, heatlines visualization, isotherms and flow rate are affected by the inclination angle of the cavity. Shirvan *et al.* (2017) investigated effects of Rayleigh number and inclination angle of insulated walls of the cavity on free convection-surface radiation heat transfer rate inside a solar cavity receiver open by the top. The square cavity is heated by the bottom at a constant flux. Computations results obtained with a SIMPLE algorithm based on the coupling of velocity-pressure fields reveal an enhancement of the heat transfer as increasing Rayleigh number and inclination angle of insulated walls.

Using the finite difference method, Bondareva *et al.* (2017) solved the problem of heatlines visualization of a free convection in a partially open rectangular cavity including a nanofluid of alumina-water with a left heat-conducting solid wall. They found that the flow heatlines are influenced by the variation of the nanofluid volume fraction. Gibanov *et al.* (2017) studied the entropy generation from a natural convection in a square open cavity packed with different porous blocks in the presence of a uniform horizontal magnetic field. The cavity opened by the top is heated by the bottom while other walls are treated adiabatic. They showed that the addition of spherical ferric oxide nanoparticles can order thermal and dynamic structures of the flow.

Via the finite volume method, Arrif *et al.* (2018) examined a natural convection in a square tilted solar cavity. It was found that isotherms and streamlines as well as heat transfer of the flow are affected by Rayleigh number, inclination of the open cavity and opening ratio of tilted solar cavity. In addition, Saleem *et al.* (2019) examined a 2D free convection in a square solar cavity receiver heated at the left vertical wall. Horizontal walls of the cavity are adiabatic while the right vertical boundary is opened. Using CFD Fluent Software, they noted a reduction of convective heat loss as increasing the cavity inclination angle from 0° to 90.

Bopche and Kumar (2019) performed an experimental study on thermal performance characteristics of a solar cavity receiver. They demonstrated that the decrease of cavity orientations from 90° to 30 conducts to reduce its performance. Then, Li *et al.* (2021) experimentally studied a concentrated solar thermal receiver for a solar heating system with seasonal storage. Various operating parameters of outlet temperature and incident power significantly affect the receiver performance. Joshi and Deore (2021) experimentally examined the inclination angle of an inverted hemispherical solar concentrator on the convective heat transfer. Optimum of the heat loss by convection is detected for a cavity angle of 90° and 0. Uzair *et al.* (2022) adopted ANSYS 16.0, CFX Solver to optimize the performance of a solar cavity shape that significantly depend on convective heat losses. They proved that the cavity receiver with conical shaped geometry performed efficiently. Behera *et al.* (2022) applied ANSYS Fluent to examine the entropy production of a natural convection in an open hemispherical cavity. For $Ra = 10^3$, a growth of the entropy generation is detected as increasing radius of curvature ratios of the hemisphere.

The design of a thermal cavity receiver is critical for the construction of solar thermal receiver and solar energy collectors. From comprehensive attempts on the available literature, it was found that no investigation has been performed on the characterization of thermal and dynamic fields as well as heat transfer of a laminar free convection evolving inside a U solar thermal cavity receiver. Therefore, the focal aim of the current research is to investigate effects of Rayleigh number ($10^3 \leq Ra \leq 10^5$), cavity orientation ($0° \leq \theta \leq 75$) and cavity aspect ratio of the cavity ranging from A = 1 to 1.75 on thermal and dynamic structures, heatlines, local and total entropy generation as well as flow rate and heat transfer of the air flow within a U solar thermal cavity receiver using SRT-BGK model of the lattice Boltzmann method. The geometrical form of a U cavity model can be assumed to be helpful for the solar thermal energy evaluation from cavity receivers in order to generate electrical energy.

2. Mathematical formulation

2.1 Physical configuration

The configuration of the current investigation depicted schematically in Figure 1 is a U cavity receiver with boundary conditions and coordinates system in X and Y directions. It is a 2D open cavity of aspect ratio A = L/H packed with an incompressible fluid of Prandtl number fixed at 0.71 and heated from bottom using three active heaters.

On Figure 1a and 1c, inclined and horizontal bottom walls of the cavity are heated at a constant temperature $T_h = 1$, vertical walls are thermally insulated while the top boundary is opened. Figure 1bpresentsthe inclined cavity for various orientations ranging from $\theta = 0°$ to 75. Length of horizontal wall, inclined wall and vertical wall is chosen as $a = \frac{L}{2}$, $b = \sqrt{\frac{a}{2}}L$ and $c = \frac{3L}{4}$, respectively. The laminar free convection flow generated by buoyancy forces is Newtonian and obeying the Boussinesq approach. To characterize thermal and dynamic fields of the flow, computations of the incompressible thermal problem by the means of SRT-BGK model of LBM are performed through Rayleigh number varying from 10^3 to 10^5, various cavity orientation ($0° \leq \theta \leq 75$) and aspect ratio of the cavity ranging from A = 1 to 1.75.

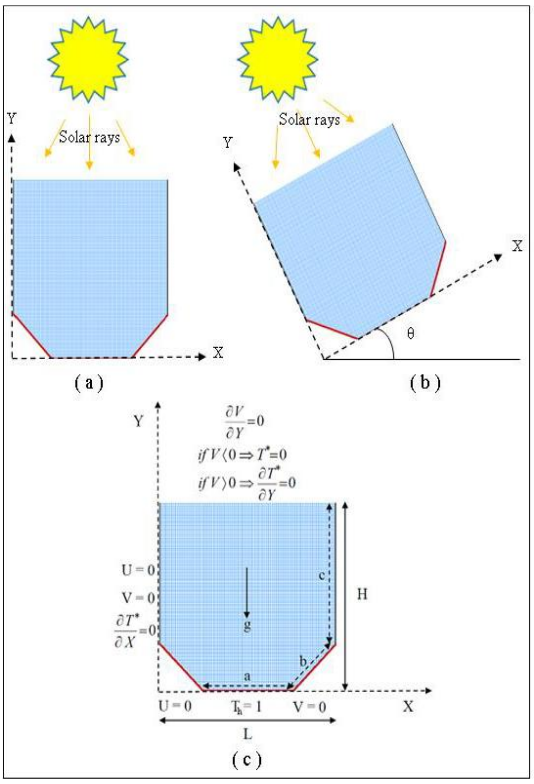

Fig 1 U solar thermal cavity receiver: (a) Horizontal and (b) inclined cavities and (c) physical configuration with boundary conditions of the problem

2.2 SRT-BGK model of Lattice Boltzmann method and boundary conditions

To predict thermal and dynamic fields of the flow as well as convective heat transfer of the considered thermal problem inside the U Solar cavity receiver, the Matlab code based on the popular Single-Relaxation-Time (SRT) with Bhatnagar-Gross-Krook (BGK) model of the Lattice Boltzmann method (LBM) is used. Numerical investigations on natural convection and heat transfer in cavities indicate that the SRT-LBM based on the BGK collision operator is a widely adopted approach for simulating fluid dynamics. The SRT-LBM model is applied in the present investigation because of its simplicity and efficiency for fluid simulation. Moreover, current results computed via this model are in line with previous data, which supports its validity in computing fluid flow problem (view section 3). Hence, this model is a reliable tool to simulate problems of convective heat transfer in semi-confined mediums. The fluid domain is discredited in uniform Cartesian cells. The LBM is based on two populations f_1 and f_2 for flow and scalar variable of temperature, respectively. They are proposed by He and Luo (1997) with SRT corresponding to the collision operator model of BGK for incompressible thermal problems. Discredited Lattice Boltzmann equations and term buoyancy force model with Boussinesq approach via BGK model are shown for flow and temperature as following:

$$f_{1_i}(x+c_i t, t+t) - f_{1_i}(x,t) = -\frac{1}{\tau_{f_1}}[f_{1i}(x,t) - f_{1i}^{eq}(x,t)] + (F_i) \quad (1)$$

$$f_{2i}(x+c_i t, t+t) - f_{2i}(x,t) = -\frac{1}{\tau_{f_2}}\left[f_{2i}(x,t) - f_{2i}^{eq}(x,t)\right] \quad (2)$$

where: f_{1i} and f_{2i} are particles distributions functions, f_{1i}^{eq} and f_{2i}^{eq} are equilibrium distributions functions for flow and temperature, respectively.

Equilibrium distributions functions corresponding to velocity W, local density ρ and temperature T^* of the flow are given as:

$$f_{1i}^{eq} = w_i\rho[1 + \frac{c_i.W}{c_s^2} + \frac{1}{2}\frac{(c_i.W)^2}{c_s^4} - \frac{1}{2}\frac{W^2}{c_s^2}] \quad (3)$$

$$f_{2i}^{eq} = w_i' T^* \left[1 + \frac{c_i W}{c_s^2}\right] \quad (4)$$

The Boussinesq approximation is applied to the external buoyancy force term. For an inclined cavity receiver, the total term force ($F_{iX} + F_{iY}$) applied to the flow is given by the following conditions:

$$F_{iX} = 3w_i(g\sin\theta)\beta T \quad \text{with X direction} \quad (5)$$

$$F_{iY} = 3w_i(g\cos\theta)\beta T \quad \text{with Y direction} \quad (6)$$

where: ΔT, g, β, W and ρ are temperature difference, gravitational acceleration, thermal expansion coefficient macroscopic velocity vector and density, respectively.
Factors of relaxation time of BGK approach for flow and temperature τ_{f_1} and τ_{f_2} corresponding to kinematic viscosity ν and thermal diffusivity χ are given as:

$$\tau_{f_1} = 3\nu + 0.5 \quad (7)$$

$$\tau_{f_2} = 2\chi + 0.5 \quad (8)$$

Speed of the sound, lattice streaming speed, lattice space and lattice time step size equal to unity, are defined by $c_s = \frac{c}{\sqrt{3}}$, $c = \frac{\Delta x}{\Delta t}$, Δt and x, respectively.

D2Q9 model of LBM used in our former investigations (Djebali *et al.* 2012, Naffouti *et al.* 2013, Naffouti *et al.* 2016, Naffouti *et al.* 2018 and Naffouti *et al.* 2020) is adopted to predict dynamic characteristics of the flow. Corresponding weighting factors w_i of D2Q9 model are defined by:

$w_0 = \frac{4}{9}$, $w_{1-4} = \frac{1}{9}$ and $w_{5-8} = \frac{1}{36}$.

Discrete velocities c_i corresponding to D2Q9 model are defined as:

$c_0 = (0,0)$, $c_{1-4} = (\pm c, 0)$ and $c_{5-8} = (\pm c, \pm c)$.

D2Q4 model of LBM applied in our previous studies (Djebali *et al.* 2012, Naffouti *et al.* 2013, Naffouti *et al.* 2016, Naffouti *et al.* 2018 and Naffouti *et al.* 2020) was used to compute the flow temperature with equal weighting factors $w_i' = 0.25$.

Macroscopic variables of W, ρ and T^* are computed by evaluating distributions functions for different directions of velocity as follows:

$$[\rho, \rho W] = \sum_{i=0}^{8}[f_{1i}, c_i f_{1i}] \quad (9)$$

$$[T^*] = \sum_{i=1}^{4}[f_{2i}] \quad (10)$$

To solve convective thermal problem of incompressible flows using SRT-BGK model of LBM, boundary conditions implementation is necessary. On solid boundaries, the D2Q9 model is adopted for Bounce-back boundary conditions (Mohamed *et al.* 2009). For a horizontal cavity receiver ($\theta = 0$), boundaries conditions corresponding to distribution functions of flow and temperature corresponding to f_1 and f_2, respectively at left vertical, south and right inclined walls of the cavity are given as:

For the left vertical wall of the cavity:

$$f_1(1,0,j) = f_1(3,0,j), f_1(5,0,j) = f_1(7,0,j), f_1(8,0,j) = f_1(6,0,j) \quad (11)$$

For the south wall of the cavity:

$$f_1(2,i,0) = f_1(4,i,0), f_1(5,i,0) = f_1(7,i,0), f_1(6,i,0) = f_1(8,i,0) \quad (12)$$

For the right inclined wall of the cavity:

$$f_1(2,i,j) = f_1(4,i,j), f_1(6,i,j) = f_1(8,i,j), f_1(3,i,j) = f_1(1,i,j) \quad (13)$$

For the horizontal hot wall of the cavity which heated isothermally at $T^* = 1$, the adopted boundary condition is given as:

$$f_2(2,i,0) = 0.5 - f_2(4,i,0) \quad (14)$$

For right inclined hot wall of the cavity which heated isothermally at $T^* = 1$, the boundary condition is defined as:

$$f_2(3,i,j) = 0.5 - f_2(1,i,j) \quad (15)$$

For adiabatic left vertical wall of the cavity, the boundary condition is evaluated by:

$$f_2(1,0,j) = f_2(3,0,j) \quad (16)$$

A special treatment of boundary conditions of flow and temperature for north open wall is necessary. The temperature is considered ambient ($T^* = 0$) if the flow is penetrating by the top of the cavity. The thermal gradient is negligible if the flow leaves the open boundary of the cavity. The same numerical procedure of boundary conditions of open cavities is adopted in previous studies (Mohamed *et al.* 2009, Mohamad 1995).

For the north boundary, the unknown density distribution of the flow is evaluated as:

$$f_1(4,i,m) = f_1(4,i,m-1) \quad (17)$$

$$f_1(7,i,m) = f_1(7,i,m-1) \quad (18)$$

$$f_1(8,i,m) = f_1(8,i,m-1) \quad (19)$$

On the north boundary, the lattice is noted as m.

The unknown density distribution of the temperature for the open boundary is determined as:

If $V < 0$ then $f_2(4,i,m) = -f_2(2,i,m)$ (20)

If $V > 0$ then $f_2(4,i,m) = f_2(4,i,m-1)$ (21)

2.3. Heatlines approach and entropy generation

To visualize energy transfer in natural convection flow, Kimura and Bejan (1983) were the first to introduce the heatlines technique. They defined the energy transfer via convection process in flow field by the sum of heat diffusion and enthalpy. Heatlines function h(x,y) which characterize the net energy flow except the surface radiation in *x* and *y* directions is given by:

$$\frac{\partial h}{\partial y} = \rho c_p w_y (T - T_0) - k\frac{\partial T}{\partial x} \quad \text{with x direction} \quad (22)$$

$$-\frac{\partial h}{\partial x} = \rho c_p w_x (T - T_0) - k\frac{\partial T}{\partial y} \quad \text{with y direction} \quad (23)$$

where ρ, k, c_p, w_x and w_y are density, thermal conductivity, specific heat, velocity components, respectively.

In the present investigation, the visualization of convective heat transfer of the flow in the cavity receiver is predicted via heatlines approach. This technique is adopted to view trajectories and distribution of heat intensity of the natural convection flow from hot to cold boundaries in flow field (Kimura and Bejan 1983). Mathematically, first derivative equations of conduction and convection heat are given as:

$$\frac{\partial H}{\partial Y} = UT^* - \frac{\partial T^*}{\partial X} \quad \text{with X direction} \quad (24)$$

$$-\frac{\partial H}{\partial X} = VT^* - \frac{\partial T^*}{\partial Y} \quad \text{with Y direction} \quad (25)$$

The equation corresponding to the visualization of dimensionless heatlines of the flow can be written as:

$$\frac{\partial^2 H}{\partial X^2} + \frac{\partial^2 H}{\partial Y^2} = \frac{\partial (UT^*)}{\partial Y} - \frac{\partial (VT^*)}{\partial X} \quad (26)$$

The local dimensionless entropy generation S_{gen} is defined as (Djebali *et al.* 2020, Shuja *et al.* 2010):

$$S_{\text{gen}} = S_{\text{gen HTI}} + S_{\text{gen FFI}} \quad (27)$$

The first term of heat transfer irreversibility is defined as:

$$S_{\text{gen HTI}} = \frac{\partial^2 T^*}{\partial X^2} + \frac{\partial^2 T^*}{\partial Y^2} \quad (28)$$

The second term of fluid friction irreversibility is given as:

$$S_{\text{gen FFI}} = \xi\left[2\left(\left(\frac{\partial U}{\partial X}\right)^2 + \left(\frac{\partial V}{\partial Y}\right)^2\right) + \left(\frac{\partial U}{\partial X} + \frac{\partial V}{\partial Y}\right)^2\right] \quad (29)$$

The irreversibility distribution ratio ξ equal to 10^{-5} is defined as:

$$\xi = \frac{\mu T_0 \alpha^2}{k(L\Delta T)^2} \quad (30)$$

The total entropy generation is obtained as (Djebali *et al.* 2020):

$$S_T = \iint S_{\text{gen}} \, dX dY \quad (31)$$

2.4 Dimensionless numbers

In the present thermal problem of the natural convection, the characteristic velocity is determined by the following equation:

$$U_c = \sqrt{g\beta\Delta TL} \quad (32)$$

After fixing characteristic velocity (U_c) and dimensionless numbers of Rayleigh and Prandtl, kinetic viscosity (ν) and thermal diffusivity (χ) of the flow inside the cavity are given as:

$$\nu = \sqrt{\frac{U_c^2 L^2}{Ra/\text{Pr}}} \quad (33)$$

$$\chi = \frac{\nu}{\text{Pr}} \quad (34)$$

Rayleigh number is defined as:

$$Ra = \frac{g\beta\Delta T L^3}{\chi\nu} \quad (35)$$

To ensure the condition related to an incompressible flow, the dimensionless number of Mach is less than 0.3.

The Mach number is given by the following equation:

$$Ma = \frac{|W|}{c_s} \quad (36)$$

where c_S and W are lattice sound speed and velocity vector, respectively.

The local Nusselt number is a considerable parameter that quantifies the heat transfer of the flow in the U cavity receiver. For the case of a horizontal cavity corresponding to the inclination angle θ = 0°, this pertinent parameter along horizontal hot wall of the cavity is defined as:

$$Nu_{Local} = \frac{3T_0^* - 4T_1^* + T_2^*}{2} \quad (37)$$

The following convergence criterion is adopted for all dependent variables at each point in the computation domain:

$$\left|\frac{\Phi(t+\Delta t)-\Phi(t)}{\Phi(t)}\right| \leq 10^{-4} \quad (38)$$

where Φ stands for a dependent variables T*, U and V.

3. Grid independence and validation of the present SRT-BGK model of LBM

3.1 Grid independence

Tests of grid independence of the present problem is conducted to specify the accurate grid size and to ensure the reliability of computations via SRT-BGK model of LBM. In the present study, the 2D open cavity is mapped with a square lattice where Δx = Δy for standards models of D2Q9 and D2Q4. Four Rayleigh number are chosen (Ra = 10^3, 10^4, 5 10^4 and 10^5) with a Prandtl number fixed at Pr = 0.71. For a Rayleigh number fixed at Ra = 5 10^4, grid refinement tests are performed for four uniform grid lattice sizes: $G_1(101^2)$, $G_2(121^2)$, $G_3(141^2)$ and $G_4(161^2)$.The Figure 2 illustrates the variation of the average Nusselt number along the horizontal hot wall of the U square cavity receiver versus Rayleigh number ($10^3 \leq Ra \leq 10^5$) for θ = 0 with different uniform grid size of lattices number ranging from 1600 to 40000. For Ra = 5 10^4, the difference for the average Nusselt number between grid sizes G_1 to G_2, G_2 to G_3 and G_3 to G_4 is 0.30%, 0.15% and 0.14%, respectively. The grid size $G_3(141^2)$ is believed to be sufficiently refined enough to simulate thermal and dynamic characteristics as well as heat transfer of the flow accurately. Consequently, findings via SRT-LBM model are taken to be grid independent. For Ra < 5 10^4 and Ra = 10^5, grid sizes of 4900 to 28900 elements were adopted, respectively.

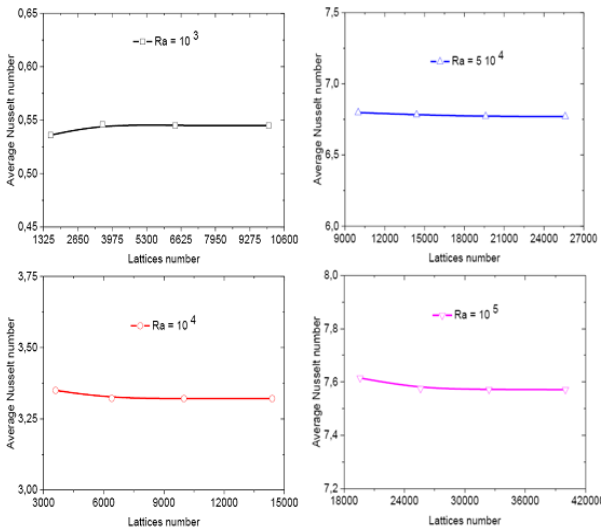

Fig 2 Effect of lattices number on the average Nusselt number along horizontal hot wall of the square cavity receiver with various Rayleigh number for θ = 0

The convergence criteria adopted here for the average Nusselt number computed along the hot wall of the cavity for θ = 0 is given as:

$$\left|\frac{\overline{Nu}(t+\Delta t)-\overline{Nu}(t)}{\overline{Nu}(t)}\right| \leq 10^{-4} \quad (39)$$

3.2 Validation of the present SRT-BGK model of LBM

To establish the credibility of the present code Matlab based on SRT-BGK model of LBM, two validations between present numerical simulations with D2Q9-D2Q4 models of LBM and former numerical simulations (Mohamed *et al.* 2009, Hussein *et al.* 2014 and Mohamad 1995) are performed. The first comparison of present predictions with those of Mohamed *et al.* (2009), Hussein *et al.* (2014) and Mohamed (1995) on convective heat transfer problems in open cavities using LBM and FVM is carried out. Figure 3 depicts a comparative study between present streamlines and isotherms of the flow and those of Mohamed *et al.* (2009) for a fixed Rayleigh number at 10^4 inside a square open cavity heated by the left wall. From Figure3, it is found an excellent agreement between present computations and those of Mohamed *et al.* (2009). Second comparison of the average Nusselt number along the hot vertical wall of the opened cavity using SRT-LBM with those of Hussein *et al.* (2014) and Mohamed (1995) is presented in Table 1. An excellent agreement is detected between results using different numerical approaches. Hence, successful validations demonstrate that suggested boundary conditions at various walls of the cavityvia current SRT-BGK model of LBM can produce reliable results of a free convection in semi-confined mediums.

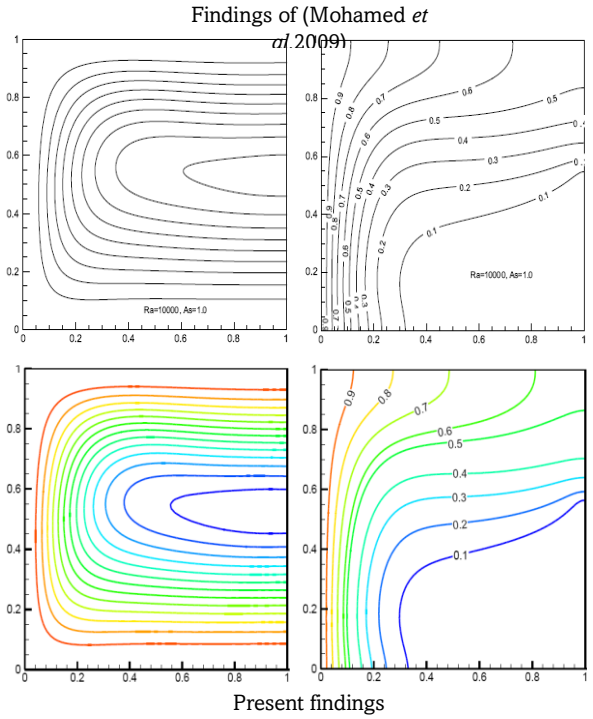

Fig 3 Comparison of present findings with those of Mohamed *et al.* 2009 inside a square open cavity for Ra = 10^4: streamlines (left) and isotherms (right)

Table 1
Comparison of present results of the average Nusselt number along the vertical hot wall of a square open cavity vs Rayleigh number with former studies (Hussein *et al.* 2014, Mohamed 1995)

	Present findings via D2Q9-D2Q4 models of LBM	Finding of (A. Hussein *et al.* 2014) via D2Q9-D2Q9 models of LBM	Finding of (Mohamed 1995) via FVM	Error (%)
Ra = 10^4	3.31	3.33	3.26	[0.6; 1.5]
Ra = 10^5	7.31	7.35	7.26	[0.5; 0.6]
Ra = 10^6	14.34	14.33	14.07	[0.07; 1.9]

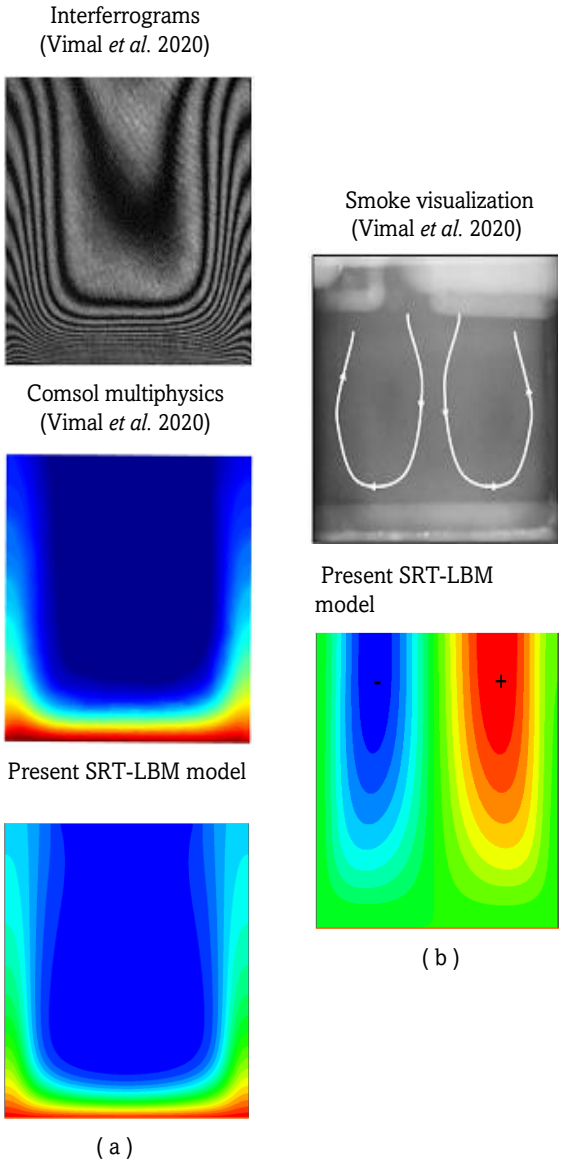

Fig 4 Comparison of present results with those of Vimal *et al.* 2020 inside a horizontal square open cavity by the top for Ra = 112076: isotherms (left) and dynamic field (right)

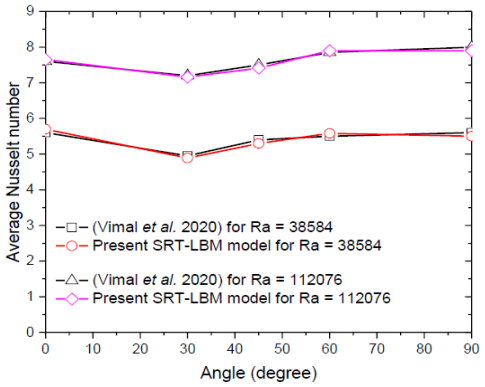

Fig 5 Comparison of present results with those of V.Kishor *et al.* 2020 of the average Nusselt number along a hot horizontal wall of a square

The ability of the current SRT-LBM model is tested on the problem predicted by Kishor *et al.* (2020) on an experimental investigation of a convective heat transfer vs the orientation of an open square horizontal cavity heated from below and opened by the top for Ra = 112076. Figures 4a and b illustrate a comparison between present computations with those of Kishor *et al.* (2020) obtained by Interferrograms, COMSOL multiphysics 5.2 and smoke visualization. From Figure4, it can be concluded an excellent agreement between results computed by the present developed SRT-LBM model and those predicted by different experimental and numerical methods adopted by Kishor *et al.* (2020). Figure5 illustrates a comparative study of the average Nusselt number computed along the hot wall for both numerical approaches versus various inclination angles of the cavity (Kishor *et al.*2020)with two values of Ra equal to 112076 and 38584. As one can remark from Figure 5, an excellent agreement is concluded for different Ra and orientation of the cavity. Consequently, these successful validations prove that the current method of LB based on the SRT-BGK model with standard D2Q9 for flow and D2Q4 for temperature is a vital tool to predict accurately and confidently the problem of the convective heat transfer within an inclined U cavity receiver as application of solar thermal energy systems. In this connection, LBM received significant attention by several researchers on computations of convective heat transfer problems owing to its accuracy, efficiency and flexibility (Ezzatneshan *et al.* 2021, Sajjadi *et al.*2021, Admi *et al.*2022, Tanabe *et al.*2023, Ren *et al.*2023, Chelia *et al.*2024 and Souai*et al.* 2025).

4. Results and discussions

Laminar free convection air flow and heat transfer are comprehensively investigated inside a U solar thermal cavity receiver through temperature and velocity distributions, heatlines visualization, entropy generation analysis, flow rate and computations of the Nusselt number. The SRT-BGK model of LBM is applied to solve current convective heat transfer problems. The air is considered as working fluid and the Prandtl number is fixed at 0.71. Physical parameters governing the considered investigation are Rayleigh number ($10^3 \leq Ra \leq 10^5$), cavity orientation ($0° \leq \theta \leq 75$) and cavity aspect ratio ($1 \leq A \leq 1.75$).

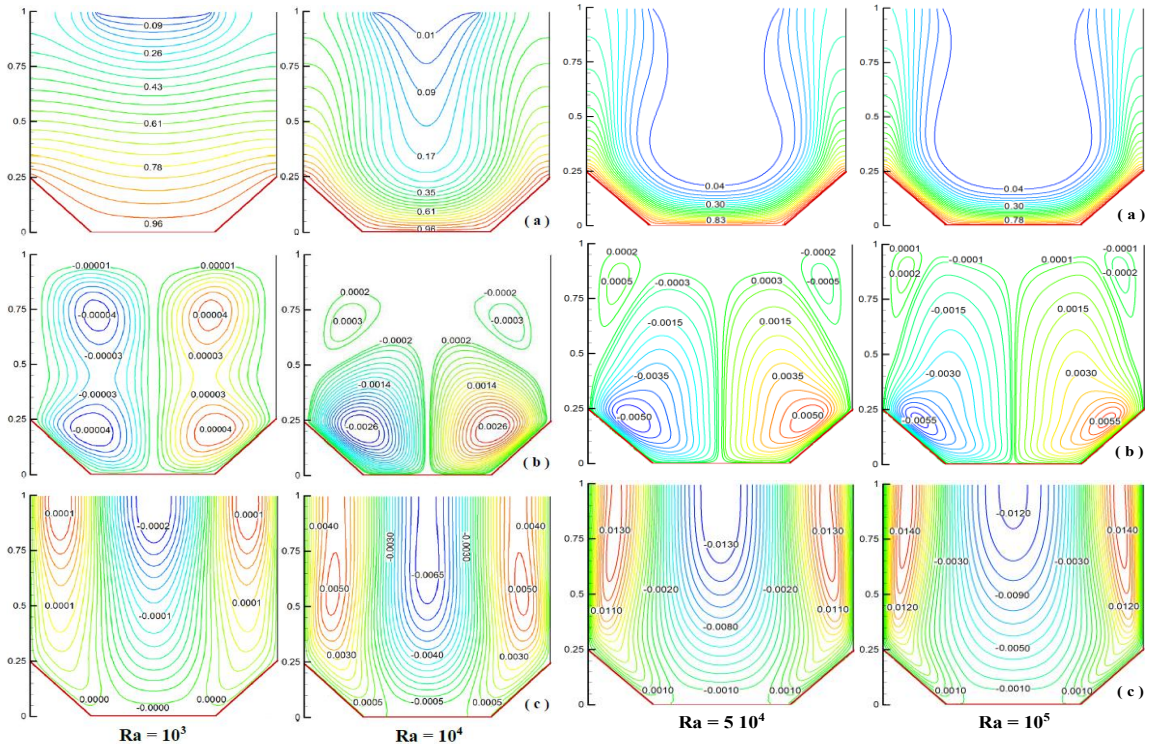

Fig 6 Isotherms (a), horizontal component (b) and vertical component (c) of the velocity of the flow in the square cavity receiver versus Ra = 10^3, 10^4, 510^4, 10^5 with θ = 0

4.1 Effect of Rayleigh number on thermal and dynamic characteristics of the flow

4.1.1 Temperature field and flow structure

Figure 6 depicts contours maps of isotherms and different components of the velocity (U and V) of the flow as a function of Rayleigh number ranging from Ra = 10^3 to 10^5. The case of a horizontal square cavity with A = 1 and θ = 0 is considered. For different values of Ra, it is shown a symmetrical behavior of thermal and dynamic fields about the mid-length of the cavity due to symmetrical boundary conditions adopted in the problem. For Ra = 10^3, the conduction effect can be seen clearly via isotherms and flow pattern. In fact, lines of thermal iso-values are approximately horizontal in the central region of the cavity with a weaker flow circulation characterized by two counter-rotating cells with a rotating anticlockwise right cell. It is due to the dominance of viscous force over buoyancy force thus indicating that the heat transfer is dissipated by conduction mode. For various Ra, contours maps of two components of the velocity show that the dynamic field of the flow is defined just by two counter-rotating cells with an intensification of flow recirculation for the growth of Ra. In addition, the rise of Ra conducts to an attenuation of the temperature of the flow in the central region of the cavity owing to the penetration of the ambient air through the top. The descending fresh air continues its path downward to symmetrically supply each thermal plume generated by an inclined hot wall. So, the flow structure is described by two symmetric contra-rotating cells with a rotating anticlockwise right cell corresponding for all Ra values. The growth of Ra leads to increase stratification degree and deformation of isotherms close to hot walls causing an increase of the thermal field intensity accompanied with an acceleration of the flow circulation for higher Ra owing to the dominance of buoyancy force over viscous forces which enhance the convective heat transfer. Moreover, the growth of Ra conducts to an intensification of the fresh air entrained by thermal plumes in the central region of the cavity. Moreover, the increase of the Ra conducts to an intensification of the vertical component of the velocity (Y-velocity) of the ambient air which goes down neighboring the vertical mid-plane of the cavity accompanied with an acceleration of the vertical ascension of the thermal plume close to the adiabatic wall. Hence, it can be noted that the convection becomes dominant over the conduction for higher Ra. On Figure 6, temperature and buoyant convection flow fields of the flow appear similar for Ra = $5{\cdot}10^4$ and 10^5. To point out effects of inclination angle and aspect ratio of the cavity receiver on thermal and dynamic characteristics as well as heat transfer of the flow, the Rayleigh number is fixed at $5{\cdot}10^4$ where the heat transfer is dominated by convection mode.

4.1.2 Vertical evolution of the energy absorbed by the flow

Figure 7 illustrates the vertical evolution of the dimensionless energy absorbed by the flow inside the horizontal

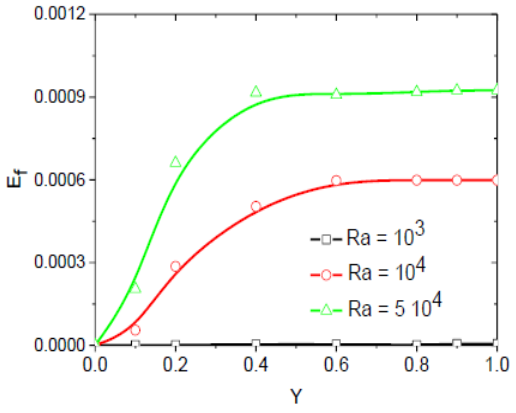

Fig 7 Vertical evolution of the dimensionless energy absorbed by the flow in the square cavity receiver as a function of Ra with θ = 0

square cavity versus Rayleigh number. The calculation of this parameter is carried out by thermal and dynamic fields of the flow. For a low Rayleigh number (Ra = 10^3), the absorption of the thermal energy is negligible because the heat transfer from hot walls is only dissipated by conduction mode. From plots, it shows an intensification of the energy as moving away from horizontal hot wall of the cavity receiver to sections Y = 0.6 and 0.5 at Ra = 10^4 and 5 10^4, respectively. It is owing to the dominance of the convective heat transfer mode over the conduction. At the upper part of the cavity, the energy remains constant for different Ra. The increase of Ra from 10^4 to $5{\cdot}10^4$cause a rise of the energy maximum about 35.14 %.

4.1.3 Heatlines visualization and distribution of local entropy generation

Kimura and Bejan, (1983) introduced the concept of heatlines technique which has been found to be useful to visualize the distribution of convective heat transfer of a fluid from hot wall to cold wall/flow. In the present study, our attention was focused on the behaviour of heatlines trajectories of the flow inside the cavity receiver. The literature shows that the analysis of heat transfer stream traces via heatlines visualization can give more information about the flow characteristics (Alireza *et al.* 2018, Ridha *et al.* 2020, Vimal *et al.* 2020, Saiful *et al.* 2022). Figure 8 illustrates heatlines and local entropy generation (S_{gen}) of the flow as a function of Ra in the square cavity with θ = 0. For all computations, symmetrical distributions of heatlines and S_{gen} about the mid-length of the cavity are shown. For Ra = 10^3, heatlines trajectories which are nearly parallel to the cavity vertical axis are directed from heaters to its exit due to the dominance of the conductive heat mode. The S_{gen} is insignificant owing to weaker heat transfer and fluid friction irreversibility.

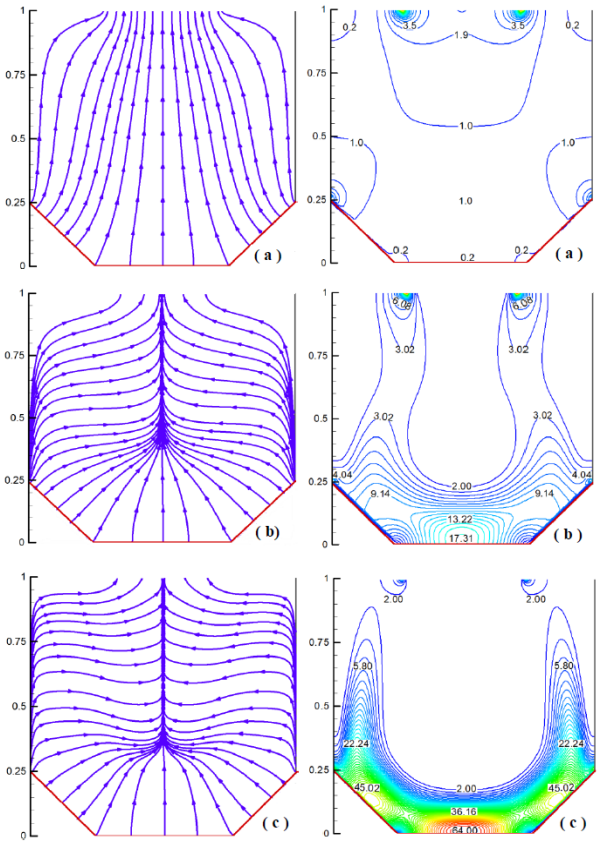

Fig 8 Heatlines visualization (top) and local entropy generation (bottom) of the flow in the square cavity receiver vs Ra for θ = 0: (a) Ra = 10^3, (b) Ra = 10^4 and (c) Ra = 5 10^4

The rise of Ra to $5{\cdot}10^4$ lead to change the direction of heatlines which becomes partially horizontal far from heaters. Additionally, heatlines trajectories which deviated toward the cavity vertical axis are tighter for a rise of Ra due to an intensification of thermal gradient and flow recirculation. The increase of Ra leads to an increase in the stratification degree of S_{gen} mainly close to heaters. Similar result was noted by Ridha *et al.* (2020) on the problem of the entropy generation of natural convection in a closed enclosure.

For Ra = 510^4, two distinct zones of heatlines and entropy generation of the flow can be identified. In the lower zone related to Y ≤ 0.25, heatlines are described by inclined trajectories converging to the mid-length of the cavity with an intense S_{gen} due to a considerable convective heat transfer and fluid friction irreversibility. In the upper zone (Y > 0.25), heatlines trajectories of the flow directed to the mid-length of the cavity receiver are almost horizontal with an attenuation of the S_{gen} near to the cavity opening.

4.2 Effect of the cavity orientation on thermal and dynamic characteristics of the flow

The study of the cavity receiver orientation can help to give more information on thermal and dynamic characteristics of the flow. In this section, all simulations in terms of vertical and transversal distributions of temperature and velocity, heatlines trajectories and entropy generation are carried out for various cavity orientations (0° ≤ θ ≤ 75) with Rayleigh number and cavity aspect ratio fixed at Ra = 5 10^4 and A = 1, respectively.

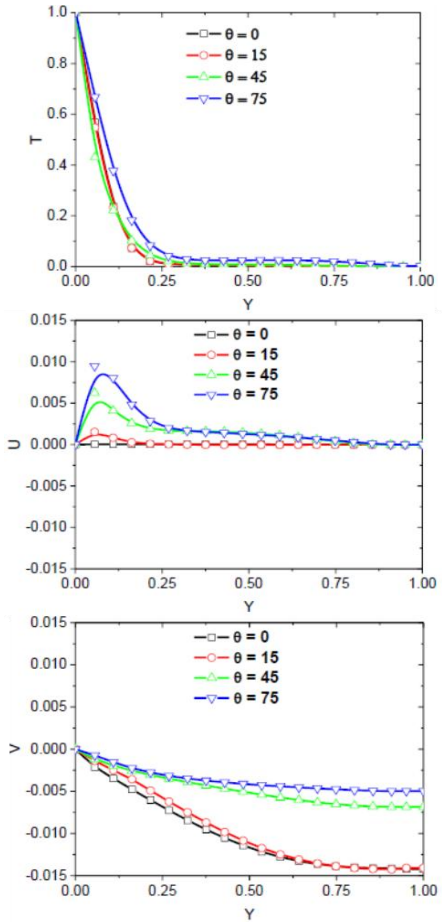

Fig 9 Vertical evolution of temperature (top), horizontal component (midle) and vertical component of the velocity (bottom) of the flow in the square cavity receiver vs cavity orientation with Ra = 5 10^4

4.2.1 Vertical evolution of temperature and velocity

Figure 9 depicts vertical evolutions of temperature and various components of the velocity (U and V) of the flow on the vertical mid-plane of the cavity receiver as a function of its orientations (θ = 0°, 15, 45 and 75). For various θ, it is found a similar behavior of thermal plots. The temperature profile is described by two different flow behaviors thus indicating the existence of two zones inside the cavity. In the first zone (Y ≤ 0.25) close to active heaters, temperature values are intense versus θ due to the persistence of thermal plumes. In this zone, it is revealed an enhancement of the flow recirculation along the horizontal direction of the positive velocity component (+X-velocity) as increasing θ thus indicating an intensification of the entrainment phenomenon of fresh air by the right thermal plume. An increase of the maximum X-velocity is shown approximately 87.34 % for the rise of θ from 15° to 75. In addition, a decrease of the negative values of the Y-velocity is observed with increasing θ thus showing a deceleration of the flow descending from the cavity opening along its vertical mid-plane. As one moves away from heaters, an attenuation of temperature is observed owing to the existence of fresh air which supply the thermal plume from below. In the second zone (Y > 0.25), temperature values approach zero and remain constant until the cavity exits owing to the existence of the ambient air which propagates toward heaters on the mid-length of the cavity. For different θ, values of X-velocity become weaker as one moves away from hot walls thus indicating a feeble flow recirculation. As the altitude of Y increases, it can be seen a growth of the magnitude of the vertical component of the velocity (Y-velocity). In the upper part of the cavity, the negative value of Y-velocity maximum decreased about 64.29 % for a reduction of cavity orientation from θ = 0° to 75, demonstrating that the flow is predominantly controlled by the Y-velocity.

4.2.2 Transversal distribution of temperature and velocity

Figure 10 presents transversal distributions of temperature and various components of the velocity of the flow versus the orientation of the square cavity receiver (0° ≤ θ ≤ 75) at two sections (Y = 0.25 and 0.75) with Ra = 5 10^4. Temperature and velocity components plot about the mid-length of the cavity show an asymmetrical behavior for various orientations except the case of θ = 0°.

Profiles related to θ = 0° show the development of the flow in two distinct zones. In the first zone (Y = 0.25) near heaters, thermal gradients and magnitude of velocity components are more intense close to vertical adiabatic walls due to the vertical ascension of each thermal plume. Above the hot horizontal wall, the temperature is lower owing to the existence of fresh air which comes from the top of the cavity to interact with each plume near the adiabatic wall. In the central region of the U cavity receiver, negative values of Y-velocity of the flow are more significant than those of X-velocity thus indicating the vertical penetration of the fresh air by the cavity opening. As increasing θ, both temperature and flow circulation decrease close to left adiabatic wall. Furthermore, an acceleration of the flow near the right adiabatic wall is observed accompanied by intense thermal gradients with increasing the cavity orientation. Hence, it can be noted that the right thermal plume becomes stronger than the left plume. In the second zone (Y = 0.75), temperature and X-velocity close to the left vertical adiabatic walls remain negligible for different θ. Positive Y-velocity values near the right adiabatic wall for different orientations of the cavity receiver are related to the vertical ascension of the right thermal plume. Meanwhile, negative values of vertical

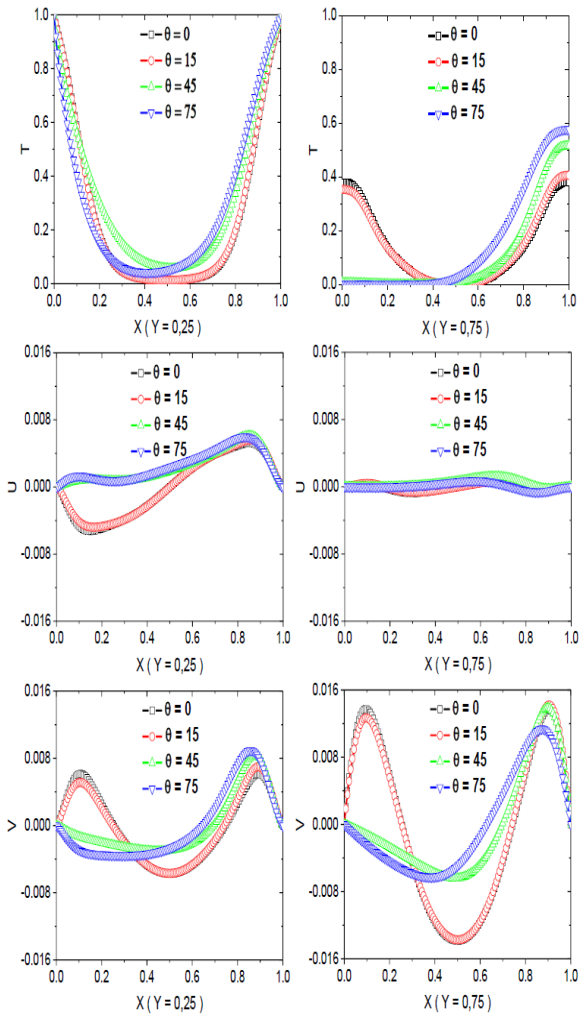

Fig 10 Transversal distribution of temperature (top), X-velocity (middle) and Y-velocity (bottom) of the flow in the square cavity of the flow vs cavity orientation for two sections (Y = 0.25 and 0.75) with Ra = 5 10^4

components of the velocity of the flow on the mid-length of the cavity are related to the penetration of the ambient air through its opening. Consequently, the rise of θ leads to decrease Y-velocity values near the left wall of the cavity with an acceleration of the flow close to the opposite adiabatic wall owing to an amplification of the right thermal plume.

4.2.3 Evolution of heatlines and local entropy generation

Figure 11 concerns heatlines visualization and distribution of entropy generation (S_{gen}) of the flow for three square cavity orientations (θ = 15°, 45 and 75) at Ra = 5 10^4. It is revealed an asymmetrical behavior of heatlines and S_{gen} about the mid-length of the cavity due to its inclination. From Figure 11a where θ = 15°, a slight deformation of heatlines trajectories toward the left adiabatic wall is observed with a decrease of the S_{gen}. The rise of θ from 0° to 75 entrains a significant deviation of the heatlines axe to the left vertical wall accompanied by a noticeable variation of the direction of their trajectories. It is further showed a decrease of the stratification degree of heatlines and S_{gen} especially close to left adiabatic wall due to weaker heat transfer and fluid friction irreversibility. This suggests that thermal gradients and flow recirculation are weaker near the left adiabatic wall compared to the opposite wall of the cavity. This behavior is related to the dominance of the right thermal plume signaled previously (see Figure 10)

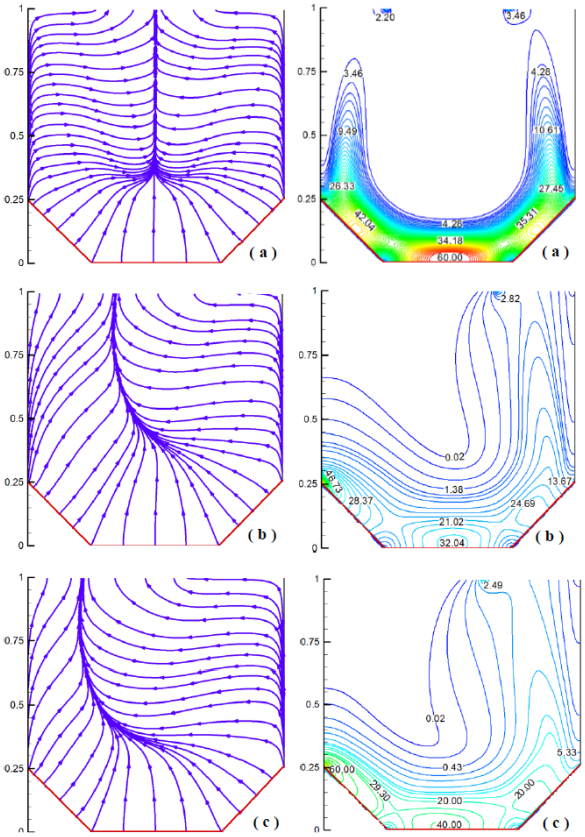

Fig 11 Heatlines visualization (left) and local entropy generation (right) of the flow for various square cavity orientations with Ra = 5 10^4: (a) θ = 15, (b) θ = 45 and (c) θ = 75

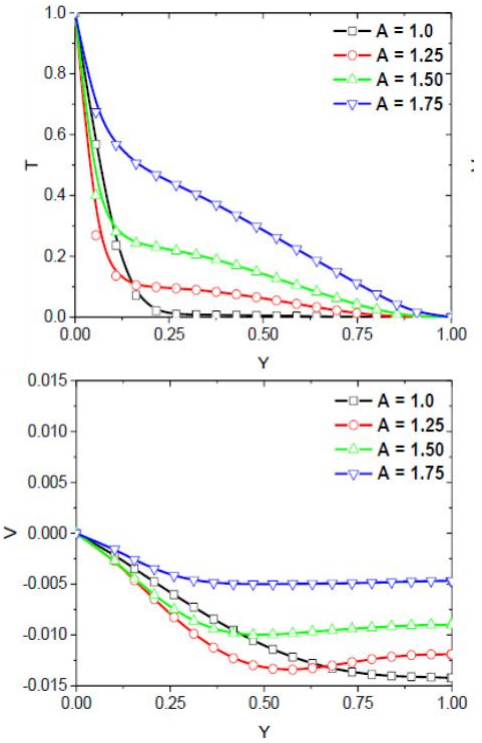

Fig 12 Vertical evolution of temperature (top) and vertical component velocity (bottom) of the flow as a function of the aspect ratio of the horizontal cavity with Ra = 5 10^4

which is described by intense temperature gradients and high magnitude of Y-velocity.

4.3 Effect of aspect ratio of the cavity on thermal and dynamic characteristic of the flow

4.3.1 Vertical evolution of temperature and velocity

Figure 12 depicts evolutions of temperature and vertical components of the velocity of the flow on the mid-length of the cavity for various aspect ratios (A = 1, 1.25, 1.5 and 1.75) with θ = 0 and Ra = 5 10^4. It is found that plots of these physical parameters are strongly affected by the variation of the geometrical parameter of the aspect ratio of the cavity.

Computational findings predicted via SRT-LBM show two behaviors of thermal and dynamic profiles thus consolidate the evolution of the flow in two distinct zones indicated previously in Figures 8-10 for Ra = 5·10^4, θ = 0 and A = 1. As one moves away from heaters, the magnitude of temperature and vertical component of the velocity decreases to remain practically constant far from cavity opening for various A. For Y ≤ 0.25 related to the first zone and near to hot walls, temperature and Y-velocity are intense as a function of A owing to a strong recirculation of thermal plumes. At section Y = 0.1 close to heaters, a rise of the temperature of about 76.9% is shown with a slight decrease of Y-velocity as increasing A from 1.25 to 1.75. In the second zone (Y > 0.25), values of temperature become weaker especially for smaller A due to the penetration of the ambient air coming from the cavity exit. At the cavity opening, it further showed a decrease of negative values of Y-velocity about 59.16% for the growth of the aspect ratio from A = 1.25 to 1.75 thus indicating a deceleration of the flow recirculation on the mid-length of the cavity toward heaters. Hence, it can be concluded that the ambient air reception by the cavity opening is weaker for higher aspect ratios.

4.3.2 Transversal distribution of temperature and vertical component velocity

Figure 13 illustrates transversal distributions of temperature and vertical component of the velocity of the flow versus the aspect ratio of the horizontal cavity (1 ≤ A ≤ 1.75) at two sections (Y = 0.25 and 0.75) with Ra = 5 10^4. A symmetrical behavior of thermal and dynamic profiles is observed for different A. These profiles present two different behaviors of the flow which consolidate its evolution into two zones. For the section Y = 0.25 located in the first zone, thermal gradients and positive values of the velocity are more intense just near adiabatic walls due to the vertical ascension of thermal plumes toward the opening cavity. With the rise of A, an intensification of the flow temperature near heaters is observed. In the central region of the cavity, the temperature is lower and the values of the vertical component of the velocity are negative by the raison of the existence of the fresh air which penetrates by the cavity opening to supply thermal plumes. At section Y = 0.75 located in the second zone, a significant rise of the temperature accompanied with a deceleration of the flow recirculation in the upper part of the cavity as increasing A thus indicating a blocking of the ascending flow especially for higher aspect ratio A = 1.75. Hence, it can be concluded that the growth of the aspect ratio of the cavity conducts to an intensification of the thermal field with a deceleration of the flow. In fact, the interaction between thermal plumes becomes significant inside the cavity as increasing A from 1 to 1.75 causing an intensification of the flow temperature and a reduction of the intensity of the entrainment phenomenon of the ambient air. Thus, the increase of the aspect ratio of the cavity receiver leads to decrease the thermal boundary layer thickness owing to the attenuation of the flow recirculation intensity.

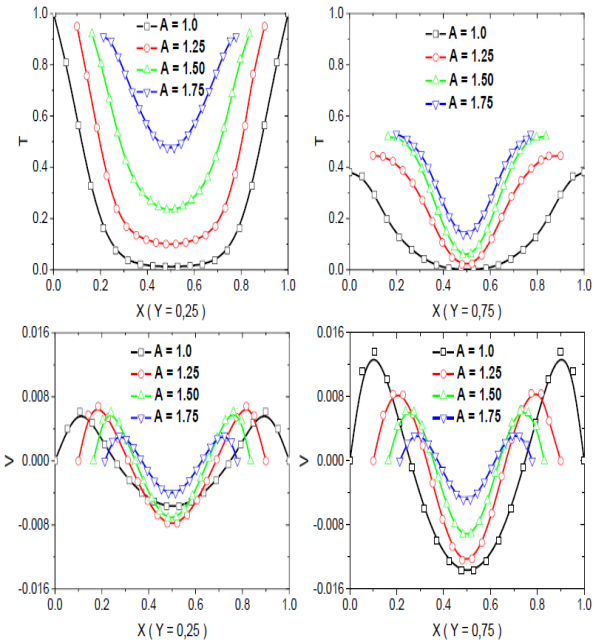

Fig 13 Transversal distribution of temperature (top) and Y-velocity (bottom) of the flow vs aspect ratio of the horizontal cavity receivec for two sections (Y = 0.25 and 0.75) with Ra = 5 10^4

4.3.3 Evolution of heatlines and local entropy generation

Figure 14 presents heatlines visualization and local entropy generation (S_{gen}) of the flow versus the aspect ratio of the horizontal cavity receiver (A = 1.25, 1.5 and 1.75) for Rayleigh number fixed at Ra = 5 10^4. For various A, heatlines and S_{gen} are characterized by symmetrical distributions related to symmetrical boundary conditions applied in this investigation. For A = 1.25, it is shown two different behaviours of heatlines and S_{gen}. Close to hot walls, a first zone (Y ≤ 0.25) is characterized by inclined heatlines centred to mid-length of the cavity with significant values of S_{gen}due to an intense convective heat transfer and fluid friction irreversibility of the flow. In the second zone far from heaters (Y > 0.25), the orientation of heatlines changes and remain almost horizontal accompanied by a decrease of the S_{gen} as getting closer to the cavity opening. As increasing A, the heatlines direction becomes more inclined thus indicating a decrease of the convective heat transfer in particularly for highest aspect ratio of the cavity. In addition, the growth of A from 1.25 to 1.75 conducts to decrease both stratification degree and magnitude of the S_{gen} inside the cavity receiver.

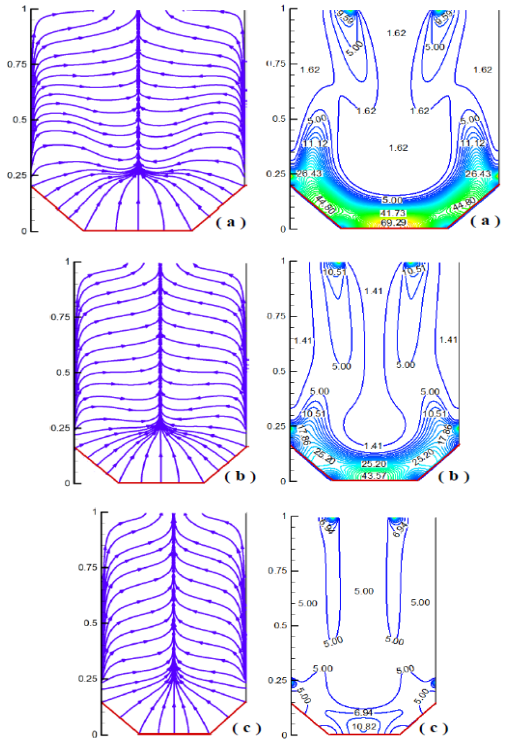

Fig 14 Heatlines visualization (left) and local entropy generation (right) of the flow for various aspect ratio of the cavity receiver with Ra = 5 10^4 and θ = 0: (a) A = 1.25, (b) A = 1.50 and (c) A = 1.75

4.4 Variation of the dimensionless flow rate

Figure 15a-c presents the evolution of flow rate (Q_v) from heaters to the opening of the U cavity receiver versus Rayleigh number (10^3 ≤ Ra ≤ 10^5), cavity orientation (0° ≤ θ≤ 75) and aspect ratio of the cavity (1 ≤ A ≤ 1.75). For the case of a horizontal square cavity related toFigure15a, Q_v is negligible at Ra = 10^3 due to a weak flow circulation mentioned here-before

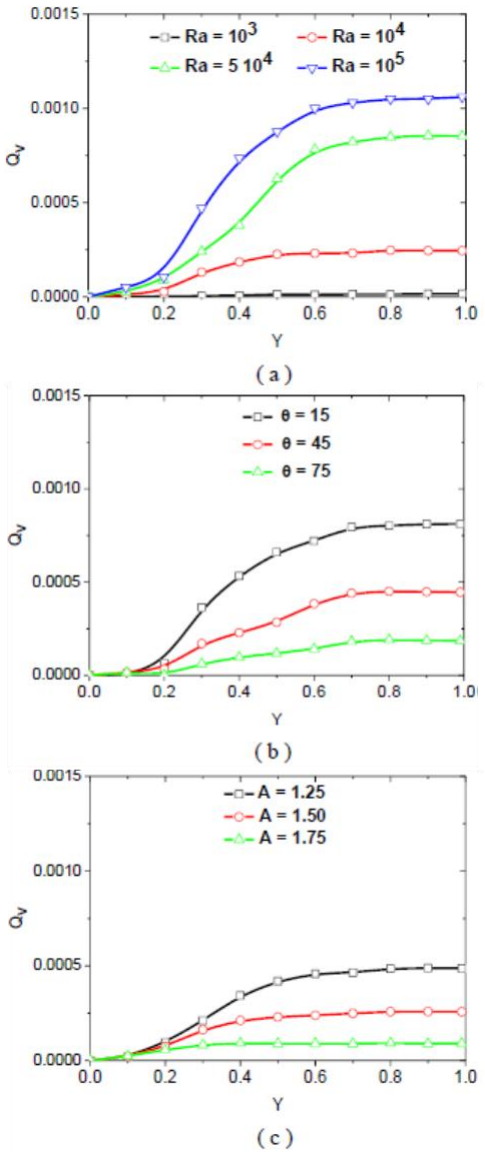

Fig 15 Evolution of the dimensionless flow rate in the cavity for various: (a) Ra with θ = 0 and A = 1, (b) θ with Ra = 5 10^4 and A= 1 and (c) A with Ra = 5 10^4 and θ = 0

in Figure 6. From plots, it is found a rise of Q_v as moving away from heaters to remain constant close to the cavity receiver for the growth of Ra from 10^4 to 10^5. In the upper region of the cavity, the increase of Rayleigh number from Ra = 10^4 to 10^5 conducts to increase the flow rate roughly 76.70 % thus showing an intensification of the entrainment phenomenon of fresh air by thermal plumes especially for higher Ra values. A similar behavior of the flow rate for various square cavity orientations at Ra = 5 10^4 is detected on Figure 15b.

The increase of the inclination angle of the U cavity receiver from θ = 15° to 75 leads to a decrease in the flow rate close to the cavity opening approximately 77.46 %. For the case of a horizontal cavity receiver at Ra = 5 10^4, plots of Figure 15 computed with SRT model of Lattice Boltzmann method demonstrate a reduction of the flow rate approximately 81.18 % with the growth of A from 1.25 to 1.75. For Ra = 5 10^4, the minimum of the flow rate is obtained for an inclined cavity receiver at 75 ° and aspect ratio equal to A = 1.75.

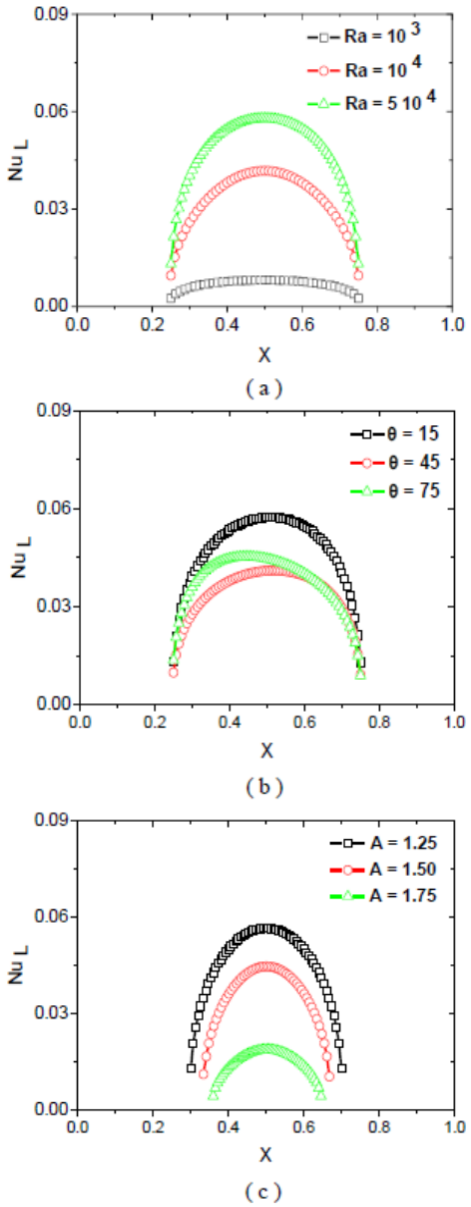

Fig 16 Variation of the local Nusselt number along the hot horizontal wall vs: (a) Ra for θ = 0 and A = 1, θ for Ra = 5 10^4 and A = 1 and (c) A for Ra = 5 10^4 and θ = 0

4.5 Optimization of convective heat transfer and total entropy generation of the flow

To point out effects of Rayleigh number (Ra), orientation (θ) and aspect ratio (A) of the cavity receiver on the heat transfer rate, a quantitative analysis of the local Nusselt number (Nu_L) along the horizontal hot wall of the cavity is depicted on Figure 16 a-c. Computations show that the convective heat transfer within the cavity is strongly affected by pertinent parameters of Ra, θ and A monitoring the current thermal problem. For the case of a horizontal square cavity (θ = 0° and A = 1), heat transfer profiles related to Figure16a are described by a symmetrical behavior for various Ra due to symmetric distribution of thermal and dynamic fields. A parabolic behavior of the local Nusselt number is observed for different Ra with a maximum on the mid-length of the cavity. The growth of Ra from 10^3 to 5 10^4 leads to enhance the heat transfer about 86 % due to the dominance of the convective mode than by conduction. On both sides of the horizontal hot wall, the Nu_L is negligible owing to the existence of weak thermal gradients between heaters of the cavity receiver where thermal plumes are generated. On the Figure 16b (Ra = 5 10^4 and A = 1), the local Nusselt number at left hot wall side is highest for various θ owing to the existence of fresh air that supply the thermal plume created by the left inclined hot wall. Figure 16b demonstrates that the heat transfer by natural convection is weakest when the cavity orientation is θ =45°. This seems to be a critical angle of the cavity receiver where the natural convection is at the minimum point. This phenomenon can be explained by referring to Figures 9 and 10. Increasing the cavity orientation from θ = 0° to 45 reduces the maximum of Nu_L roughly 29.31 % owing to an attenuation of thermal gradients and slowdown of the flow circulation. A slight increase of the local Nusselt-number, about 6.89%, is detected when the cavity orientation rises from θ = 45° to 75. Based on Figure 16c related to a U horizontal cavity where θ = 0°and Ra = 5 10^4, it is shown a decrease of the maximum of the local Nusselt number on the mid-length of the cavity about 68.96 % with the rise of A from 1 to 1.75. This considerable reduction of the heat transfer is attributed to the intensification of the thermal filed and the decrease of the flow recirculation detected previously in Figure 13 for A = 1.75.Next investigation is concentrated on the optimization of heat transfer quantified by the average Nusselt number (Nu*) along the horizontal hot wall of the cavity receiver and total entropy generation (S_T) of the flow which may be to help to enhance the efficiency of solar thermal energy systems such as solar collectors. The study of significant engineering parameters of Nu* and S_T versus Rayleigh number, angle and aspect ratio of the cavity receiver can explains the behavior of the heat transfer by natural convection convective of the flow inside the cavity.

Figure 17 illustrates variations of average Nusselt number and total entropy generation us a function of Rayleigh number from 10^3 to 10^5, cavity orientation from 0° to 75 and aspect ratio of the cavity from A = 1 to 1.75. Figure 17a, which depicts the variation of Nu* versus Rayleigh number for a horizontal square cavity, reveals two modes of heat transfer. For Ra = 10^3, the average Nusselt number is equal to 1 due to the dominance of the conduction process. Beyond Ra = 10^3, a fast rise of the average Nusselt number approximately 88% is detected as increasing Rayleigh-number thus showing an enhancement of the heat transfer through natural convection. Furthermore, the increase of Rayleigh number conducts to a growth of the total entropy generation roughly 61% from Ra = 10^4 to 10^5 owing to an intensification of both the value of heat transfer irreversibility and fluid friction irreversibility. For higher Rayleigh number, the total entropy generation becomes substantial by the raison of

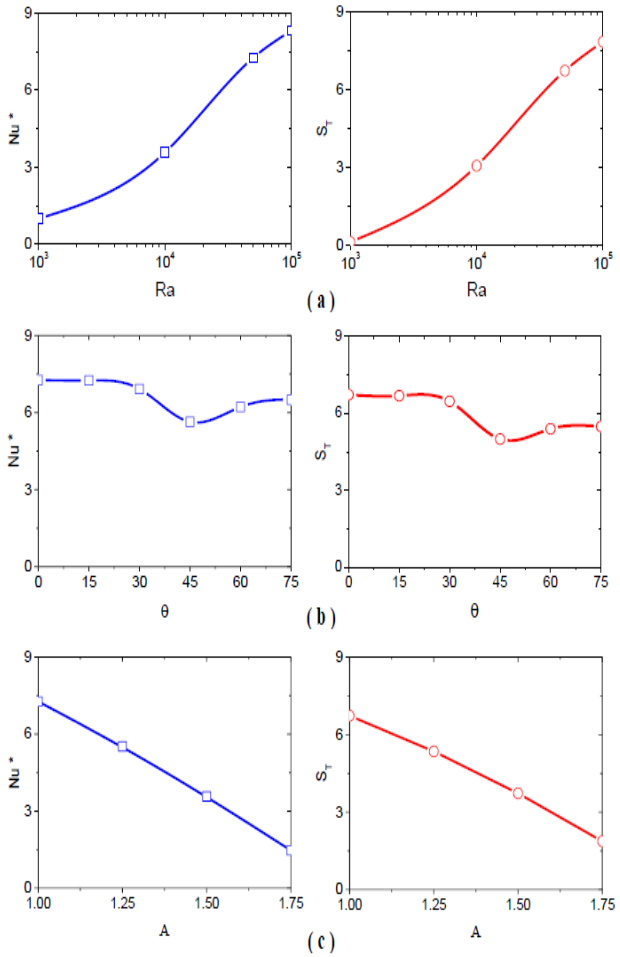

Fig 17 Variation of the average Nusselt number along the hot horizontal wall (left) and total entropy generation (right) vs:(a) Ra for θ = 0 and A = 1, (b) θ for Ra = 5 10^4 (b) and A = 1 and (c) A for Ra = 5 10^4 and θ = 0

the presence of intense thermal and dynamic gradients of the flow. Consequently, it can be deduced that the flow is predominantly governed by the natural convection for Ra = 5 10^4 and 10^5.

Figure 17b depicts variations of average Nusselt number and total entropy generation of the flow versus cavity orientation for Ra = 5 10^4. It can be observed the existence of an optimum of Nu* and S_T for the same orientation of the cavity receiver evaluated at θ = 45°. With the growth of the cavity orientation from θ = 0° to 22, values of the average Nusselt number remain constant at 7.26 and then it decreases as a function of θ around 22.72% to attain its minimum at θ = 45°. A rise of the average Nusselt number roughly 13.60 % is detected as increasing cavity orientation from 45° to 75 due to an intensification of the X-component of the buoyancy force. A similar behavior of S_T is observed for the rise of θ from 0° to 75. The critical cavity orientation at θ = 45° related to the lowest values of average Nusselt number and total entropy generation of the flow is linked to a weaker fluid friction irreversibility thus demonstrating an attenuation of the convective heat transfer of the flow. At this angle θ = 45°, the Y-component of the buoyancy force is equal in magnitude to the X-component. Hence, it can be noted that the orientation of the cavity receiver at θ = 45° is adequate to store the maximum of the thermal energy such as solar collectors. Figure 17c presents variations of average Nusselt number and total entropy generation of the flow as a function of the aspect ratio of the cavity receiver at Ra = 5 $10^4$and for the case of a horizontal cavity. The growth of the aspect ratio of the cavity receiver from A = 1 to 1.75 entrains a linear reduction of the average Nusselt number about 80.76 % and a decrease of the total entropy generation about 72 % owing to a deceleration of the flow circulation thus indicating a decrease of the heat transfer by convection mode. These results are consistent with temperature and flow patterns signaled previously in Figures 12 and 13. Consequently, it can be concluded that minimum values of Nu* and S_T are detected simultaneously for highest aspect ratio of the inclined cavity and at critical cavity orientation (θ = 45°) for Ra = 5 10^4.

5. Conclusion

In the current paper, a comprehensive lattice Boltzmann study is performed on convective heat transfer in a U cavity receiver. Solar thermal energy systems applications have provided a major incentive for this research owing to the significance of convective heat transfer in passive solar thermal receiver or energy collectors. This numerical investigation aims to elucidate effects of Rayleigh number (Ra), cavity receiver orientation (θ) and cavity aspect ratio (A) on fluid flow and heat transfer mechanisms. Results of this research can contribute to improving performances of solar heating systems. It is found a symmetrical behavior of the air flow for various Ra and A owing to symmetrical boundary conditions adopted in the problem. This investigation shows thatSRT-BGK model of LBM is validated with previous works and good agreements are achieved. This approach based on D2Q9-D2Q4 models is shown to be a reliable tool to simulate problems of convective heat transfer in semi-confined mediums like solar thermal cavity receivers. The rise of Ra entrains a growth of thermal and dynamic gradients of the flow owing to an intensification of the entrainment of fresh air by thermal plumes in the central region of the horizontal square cavity. As a result, the convection becomes more dominant than the conduction causing a rise of the energy maximum absorbed by the flow about 35.14 % as Ra increases from 10^4 to 5 10^4. With the rise of Ra, heatlines trajectories deviated to the mid-length of the cavity are tighter and the stratification degree of S_{gen} becomes higher close to heaters.

For various orientations of the square cavity at Ra = 5 10^4, the analysis of flow patterns, heatlines and S_{gen} reveals the development of the flow in two different zones within the horizontal square cavity. The first zone (Y ≤ 0.25) is described by intense thermal and dynamic gradients with inclined heatlines trajectories directed to the mid-length of the cavity and high values of the local entropy generation. In the second zone (Y > 0.25), an attenuation of temperature, S_{gen} and velocity of the flow is detected and heatlines trajectories become nearly horizontal. The rise of the cavity orientation from θ = 0° to 75 decreases the stratification degree of heatlines and S_{gen} near the left adiabatic wall owing to weaker fluid friction irreversibility.As increasing the horizontal cavity aspect ratio at Ra = 5 10^4, a significant increase of temperature values is observed with a deceleration of Y-component of the velocity due the blocking of the ascending flow mainly for higher aspect ratio of A = 1.75. The rise of aspect ratio of the cavity decreases stratification degree and magnitude of S_{gen} with a change of the heatlines direction which becomes more inclined. On the other hand, the increase of Ra from 10^4 to 10^5 causes a rise of the flow rate about 76.70 % at the upper region of the horizontal square cavity due to an intensification of the entrainment phenomenon of fresh air by thermal plumes for higher Ra values. Conversely, a reduction of the flow rate of about 77.46 % and 81.18 % is detected when θ increases from 15° to 75 and A from 1.25 to 1.75, respectively.

For Ra = 5 10^4, the optimization of the convective heat transfer reveals that minimum values of average Nusselt

number and total entropy generation are detected for higher aspect ratio of the inclined cavity receiver at θ = 45°. This cavity orientation related to the insignificant convective heat transfer is adequate to store the maximum of the thermal energy inside solar receiver systems.

References

Admi, Y., Moussaoui, M. A., &Mezrhab, A. (2022). Numerical investigation of convective heat transfer and fluid flow past a three square cylinders controlled by a partition in channel. *International Journal of Renewable Energy Development*, *11*, 766–781; https://doi.org/10.14710/ijred.2022.43790

Arrif, T., Chehhat, A., Abo-Serie, E., & Benchabane, A. (2018). Numerical study of natural convection in square tilted solar cavity considering extended domain. *FDMP*, *14*(4), 223–242; https://doi.org/10.1016/j.jmmm.2017.12.075

Aydin, O., & Yang, J. (2000). Natural convection in enclosure with localized heating from below and symmetrically cooling from sides. *International Journal of Numerical Methods for Heat & Fluid Flow*, *10*(5), 518–529; https://doi.org/10.1108/09615530010338196

Azwadi, C. S. N., Razzaghian, M., Pourtousi, M., &Safdari, A. (2013). Numerical prediction of free convection in an open-ended enclosure using lattice Boltzmann method. *International Journal of Mechanical and Materials Engineering*, *8*(1), 58–62 ; https://doi.org/10.1016/j.ijthermalsci.2009.02.004.

Behera, B. R., Chandrakar, V., Mukherjee, A., & Senapati, J. R. (2022). Entropy production analysis and cooling time calculation for an open hemispherical cavity in natural convection. *Journal of Process Mechanical Engineering*, *237*(4). https://doi.org/10.1177/09544089221117142

Bondareva, N. S., Sheremet, M. A., &Öztop, H. F. (2017). Heatline visualization of natural convection in a thick-walled open cavity filled with a nanofluid. *International Journal of Heat and Mass Transfer*, *109*, 175–186; https://doi.org/10.1016/j.ijheatmasstransfer.2017.01.124

Bondareva, N. S., Sheremet, M. A., Öztop, H. F., & Abu-Hamdeh, N. (2016). Heatline visualization of MHD natural convection in an inclined wavy open porous cavity filled with a nanofluid with a local heater. *International Journal of Heat and Mass Transfer*, *99*, 872–881; https://doi.org/10.1016/j.ijheatmasstransfer.2016.04.055

Bopche, S. B., & Kumar, S. (2019). Experimental investigations on thermal performance characteristics of a solar cavity receiver. *International Journal of Energy and Environmental Engineering*, *10*, 463–481; https://doi.org/10.1007/s40095-019-00321-4

Chelia, W., Laouer, A., &Mezaache, E. H. (2024). LBM simulation of free convection heat transfer of Cu/Water nanofluid in inclined cavity with non-uniform heating temperature distribution. *Journal of Nanofluids*, *13*, 553–562; https://doi.org/10.1166/jon.2024.2135

Djebali, R., ElGanaoui, M., &Naffouti, T. (2012). A 2D lattice Boltzmann full analysis of MHD convective heat transfer in saturated porous square enclosure. *Computer Modeling in Engineering and Sciences*, *84*, 499–527; https://doi.org/10.3970/cmes.2012.084.499

Djebali, R., Jaouabi, A., Naffouti, T., &Abboudi, S. (2020). Accurate LBM appraising of pin-fins heat dissipation performance and entropy generation in enclosures as application to power electronic cooling. *International Journal of Numerical Methods for Heat and Fluid Flow*, *30*(2), 742–768; https://www.emerald.com/insight/content/doi/10.1108/hff-01-2019-0006/full/html

Ezzatneshan, E., Salehi, A., &Vaseghnia, H. (2021). Study on forcing schemes in the thermal lattice Boltzmann method for simulation of natural convection flow problems. *Journal of Heat Transfer*, *50*, 7604–7631; https://doi.org/10.1002/htj.22245

Fontana, É., Silva, A. D., & Mariani, V. C. (2011). Natural convection in a partially open square cavity with internal heat source: An analysis of the opening mass flow. *International Journal of Heat and Mass Transfer*, *54*, 1369–1386; https://doi.org/10.1016/j.ijheatmasstransfer.2010.11.053

Ghazouani, K., Skouri, S., Bouadila, S., &Guizani, A. A. (2019). Thermal optimization of solar dish collector for indirect vapor generation. *International Journal of Energy Research*, *43*, 7240–7253; https://doi.org/10.1002/er.4748

Gibanov, N. S., Sheremet, M., Öztop, H. F., & Al-Salem, K. (2017). MHD natural convection and entropy generation in an open cavity having different horizontal porous blocks saturated with a ferrofluid. *Journal of Magnetism and Magnetic Materials*.

Haghshenas, A., Rafati Nasr, M., & Rahimian, M. H. (2010). Numerical simulation of natural convection in an open-ended square cavity filled with porous medium by lattice Boltzmann method. *International Communications in Heat and Mass Transfer*, *37*, 1513–1519; https://doi.org/10.1016/j.icheatmasstransfer.2010.08.006

Hassan, A., Quanfang, C., Abbas, S., Lu, W., &Youming, L. (2021). An experimental investigation on thermal and optical analysis of cylindrical and conical cavity copper tube receivers design for solar dish concentrator. *Renewable Energy*, *179*, 1849–1864; https://doi.org/10.1016/j.renene.2021.07.145

He, X., & Luo, L. S. (1997). Lattice Boltzmann model for the incompressible Navier-Stokes equation. *Journal of Statistical Physics*, *88*, 927–944; https://ui.adsabs.harvard.edu/link_gateway/1997JSP....88..927H/doi:10.1023/B:JOSS.0000015179.12689.e4

Huang, W., Huang, F., Hu, P., & Chen, Z. (2013). Prediction and optimization of the performance of parabolic solar dish concentrator with sphere receiver using analytical function. *Renewable Energy*, *53*, 18–26; https://doi.org/10.1016/j.renene.2012.10.046

Hussein, A. K., Ashorynejad, H. R., Shikholeslami, M., &Sivasankaran, S. (2014). Lattice Boltzmann simulation of natural convection heat transfer in an open enclosure filled with Cu–water nanofluid in a presence of magnetic field. *Nuclear Engineering and Design*, *268*, 10–17; https://doi.org/10.1016/j.nucengdes.2013.11.072

Islam, S., Bairagi, T., Islam, T., Rana, B. M. J., Reza-E-Rabbi, S. K., & Rahman, M. M. (2022). Heatline visualization in hydromagnetic natural convection flow inside a prismatic heat exchanger using nanofluid. *International Journal of Thermofluids*, *16*, 1–12; https://doi.org/10.1016/j.ijft.2022.100248

Joshi, A., &Deore, E. R. (2021). Performance characteristics of heat loss of the inverted hemispherical solar concentrator receiver. *International Journal of Applied Research*, *7*(3), 221–225; http://dx.doi.org/10.22271/allresearch.2021.v7.i3d.8400

Kim, S. J., & Lee, S. W. (1996). *Air cooling technology for electronic equipment*. Boca Raton, FL: CRC Press.

Kimura, S., & Bejan, A. (1983). The heatline visualization of convective heat transfer. *Journal of Heat Transfer*, *105*(4), 916–919; https://doi.org/10.1115/1.3245684

Kishor, V., Kumar, R., Singh, S., & Srivastava, A. (2020). Non-intrusive experimental study of natural convection in open square cavity at different inclinations. *Journal of Flow Visualization and Image Processing*, *27*, 333–357; https://doi.org/10.1615/JFlowVisImageProc.2020031075

Kumar, A., Joshi, J. B., & Nayak, A. K. (2017). A comparison of thermal-hydraulic performance of various fin patterns using 3D CFD simulations. *International Journal of Heat and Mass Transfer*, *109*, 336–356; https://doi.org/10.1016/j.ijheatmasstransfer.2017.01.102

Li, X., Wang, Z., Li, J., Chen, L., Bai, Y., Yang, M., Guo, M., Sun, F., & Yuan, G. (2021). Numerical and experimental study of a concentrated solar thermal receiver for a solar heating system with seasonal storage. *International Journal of Energy Research*, *45*, 7588–7604; https://doi.org/10.1002/er.6341

Liu, D., Xin-Feng, L., Bo, L., Si-Quan, Z., & Yan, X. (2018). Progress in thermochemical energy storage for concentrated solar power: A review. *International Journal of Energy Research*, *42*, 4546–4561; https://doi.org/10.1002/er.4183

Loni, R., Kasaeian, A. B., Asli-Ardeh, E. A., Ghobadian, B., & Gorjian, Sh. (2018). Experimental and numerical study on dish concentrator with cubical and cylindrical cavity receivers using thermal oil. *Energy*, *154*, 168–181; https://doi.org/10.1016/j.energy.2018.04.102

Mahmoudi, A. H., Shahi, M., &Talebi, F. (2012). Entropy generation due to natural convection in a partially open cavity with a thin heat source subjected to a nanofluid. *Numerical Heat Transfer: Part A—Applications*, 283–305; https://doi.org/10.1080/10407782.2012.647990

McGarry, M., & Kohl, J. G. (2013). Analysis of dual heat sources in a partially open enclosure. *Advances in Mechanical Engineering*, *2013*, 126353; https://doi.org/10.1155/2013/126353

Mohamad, A. A. (1995). Natural convection in open cavities and slots. *Numerical Heat Transfer*, *27*, 705–716 ; https://doi.org/10.1080/10407789508913727

Mohamed, A. A., Elganaoui, M., & Bennacer, R. (2009). Lattice Boltzmann simulation of natural convection in an open ended cavity. *International Journal of Thermal Sciences*, *48*, 1870–1876; https://doi.org/10.1016/j.ijthermalsci.2009.02.004

Naffouti, T., Thamri, L., &Djebali, R. (2020). Heat transfer optimization of MHD convection in enclosure heated with heaters separated by an active triangular body via SRT-BGK model. *International Journal of Engineering Science Invention*, *9*, 28–50; https://www.ijesi.org/papers/Vol(9)i9/Ser-2/D0909022850.pdf

Naffouti, T., Thamri, L., Naffouti, A., &Zinoubi, J. (2018). Optimization of convective heat transfer from two heating generators into horizontal enclosure including a discrete obstacle: A lattice Boltzmann comprehensive investigation. *Journal of Applied Fluid Mechanics*, *11*(5), 1277–1286; https://doi.org/10.29252/jafm.11.05.28614

Naffouti, T., Zinoubi, J., & Ben Maad, R. (2013). Lattice Boltzmann analysis of 2-D natural convection flow and heat transfer within square enclosure including an isothermal hot block. *International Journal of Thermal Technologies*, *3*(4), 146–154; https://inpressco.com/lattice-boltzmann-analysis-of-2-d-natural-convection-flow-and-heat-transfer-within-square-enclosure-including-an-isothermal-hot-block/

Naffouti, T., Zinoubi, J., Che Sidik, N. A., & Ben Maad, R. (2016). Applied thermal lattice Boltzmann model for fluid flow of free convection in 2-D enclosure with localized two active blocks: Heat transfer optimization. *Journal of Applied Fluid Mechanics*, *9*(1), 419–430; https://doi.org/10.18869/acadpub.jafm.68.224.24198

Nayak, J., Agrawal, M., Mishra, S., Sahoo, S. S., Swain, R. K., & Mishra, A. (2018). Combined heat loss analysis of trapezoidal shaped solar cooker cavity using computational approach. *Case Studies in Thermal Engineering*, *12*, 94–103; https://doi.org/10.1016/j.csite.2018.03.009

Novozhilova, A. V., Maryna, Z. G., Samorodov, A. V., & Lvov, E. A. (2017). Research of heat transfer of staggered horizontal bundles of finned tubes at free air convection. *Journal of Physics: Conference Series*, *891*(1), 012056 ; https://ui.adsabs.harvard.edu/link_gateway/2017JPhCS.891a2056N/doi:10.1088/1742-6596/891/1/012056

Ophoff, C., Abuseada, M., Ozalp, N., & Moens, D. (2020). Systematic approach for design optimization of a 3 kW solar cavity receiver via multiphysics analysis. *Solar Energy*, *206*, 420–435; https://doi.org/10.1016/j.solener.2020.06.021

Pavlovic, S., Loni, R., Bellos, E., Vasiljevi, D., Najafi, G., &Kasaeian, A. (2018). Comparative study of spiral and conical cavity receivers for a solar dish collector. *Energy Conversion and Management*, *178*, 111–122 ; https://doi.org/10.1016/j.enconman.2018.10.030

Peterson, G. P., & Ortega, A. (1990). Thermal control of electronic equipment and devices. *Advances in Heat Transfer, 20*, 181–214; https://doi.org/10.1016/S0065-2717(08)70028-5

Prakash, M. (2014). Numerical study of natural convection heat loss from cylindrical solar cavity receivers. *ISRN Renewable Energy*, *2014*, 104686; https://doi.org/10.1155/2014/104686

Prasad, D. R., Senthilkumar, R., Lakshmanarao, G., Krishnan, S., & Prasad, B. N. (2019). A critical review on thermal energy storage materials and systems for solar applications. *AIMS Energy*, *7*, 507–526; https://doi.org/10.3934/energy.2019.4.507

Rahimi, A., Sepehr, M., JanghorbanLariche, M., Mesbah, M., Kasaeipoor, A., & Hasani Malekshah, E. (2018). Analysis of natural convection in nanofluid-filled H-shaped cavity by entropy generation and heatline visualization using lattice Boltzmann method. *Physica E: Low-dimensional Systems and Nanostructures*, *97*, 347–362; https://doi.org/10.1016/j.physe.2017.12.003

Ren, X., Liu, F., & Xin, Z. (2023). A novel thermal lattice Boltzmann method for numerical simulation of natural convection of non-Newtonian fluids. *Process*, *8*, 1–16; https://doi.org/10.3390/pr11082326

Sadat, H. (2022). A simple analytical thermal model of solar cavity receivers. *Thermal Science and Engineering Progress*, *29*, 101223; https://doi.org/10.1016/j.tsep.2022.101223

Sajjadi, H., Amiri Delouei, A., Mohebbi, R., Izadi, M., &Succi, S. (2021). Natural convection heat transfer in a porous cavity with sinusoidal temperature distribution using Cu/Water nanofluid: Double MRT lattice Boltzmann method. *Communications in ComputationalPhysics*, *29*, 292–318; https://doi.org/10.4208/cicp.OA-2020-0001

Saleem, H., Nizamani, A. H., Bhutto, W. A., Soomro, A. M., Soomro, M. Y., & Toufik, A. (2019). Two dimensional natural convection heat losses from square solar cavity receiver. *IJCSNS International Journal of Computer Science and Network Security*, *19*(4); http://paper.ijcsns.org/07_book/201904/20190441.pdf

Shirvan, K. M., Mamourian, M., Mirzakhanlari, S., &Ellahi, R. (2017). Numerical study of surface radiation and combined natural convection heat transfer in a solar cavity receiver. *International Journal of Numerical Methods for Heat & Fluid Flow*, *27*(10), 2385–2399; https://doi.org/10.1108/HFF-10-2016-0419

Shirvan, K. M., Mamourian, M., Mirzakhanlari, S., Rahimi, A. B., &Ellahi, R. (2017). Numerical study of surface radiation and combined natural convection heat transfer in a solar cavity receiver. *International Journal of Numerical Methods for Heat & Fluid Flow*, *27*(10), 2385–2399; https://doi.org/10.1108/HFF-10-2016-0419

Shuja, S., Yilbas, B., & Kassas, M. (2010). Entropy generation in a square cavity: Effect of porous block configurations in relation to cooling applications. *International Journal of Numerical Methods for Heat and Fluid Flow*, *20*(3), 332–347; https://www.emerald.com/insight/content/doi/10.1108/09615531011024075/full/html

Souai, S., Trabelsi, S., &Sediki, E. (2025). LBM simulation for combined thermal radiation and natural convection in 2D enclosure with multiple solid blocks. *Numerical Heat Transfer, Part A: Applications*, *86*, 1160–1185; https://doi.org/10.1080/10407782.2023.2272792

Tanabe, Y., Yaji, K., & Ushijima, K. (2023). Topology optimization using the lattice Boltzmann method for unsteady natural convection problems. *Structural and Multidisciplinary Optimization*, *66*, 1–22; https://doi.org/10.1007/s00158-023-03522-y

Tian, Y., & Zhao, C. (2013). A review of solar collectors and thermal energy storage in solar thermal applications. *Applied Energy*, *104*, 538–553; https://doi.org/10.1016/j.apenergy.2012.11.051

Unger, S., Beyer, M., &Szalinski, L. (2020). Thermal and flow performance of tilted oval tubes with novel fin designs. *International Journal of Heat and Mass Transfer*, *153*, 1–12; https://doi.org/10.1016/j.ijheatmasstransfer.2020.119621

Unger, S., Beyer, M., Gruber, S., & Willner, R. (2019). Experimental study on the air-side thermal-flow performance of additively manufactured heat exchangers with novel fin designs. *International Journal of Thermal Sciences*, *146*, 106074; https://doi.org/10.1016/j.ijthermalsci.2019.106074

Uzair, M., Chaudhary, G. Q., Rehman, N. U., Anwer, M. Z., Hassan, S. H., Siddiqui, H., & Hussain, M. S. (2022). Numerical investigation to determine the optimized solar cavity shape. *GMSARN International Journal*, *16*, 55–65; https://gmsarnjournal.com/home/wp-content/uploads/2021/05/vol16no1-6.pdf

Venkatachalam, T., & Cheralathan, M. (2019). Effect of aspect ratio on thermal performance of cavity receiver for solar parabolic dish concentrator: An experimental study. *Renewable Energy*, *139*, 573–581; https://doi.org/10.1016/j.renene.2019.02.102

Wu, Z., Dai, W., Man, M., & Luo, E. (2012). A solar-powered traveling-wave thermoacoustic electricity generator. *Solar Energy*, *86*, 2376–2382; https://doi.org/10.1016/j.solener.2012.05.010